





# In vitro maturation and in vivo stability of bioprinted human nasal cartilage

Xiaoyi Lan<sup>1</sup>, Yan Liang<sup>2</sup>, Margaret Vyhldal<sup>2</sup> ,  
Esra JN Erkut<sup>2</sup>, Melanie Kunze<sup>2</sup>, Ailette Mulet-Sierra<sup>2</sup>,  
Martin Osswald<sup>3,4</sup>, Khalid Ansari<sup>4</sup>, Hadi Seikaly<sup>4</sup>,  
Yaman Boluk<sup>1</sup> and Adetola B Adesida<sup>2,4</sup> 

## Abstract

The removal of skin cancer lesions on the nose often results in the loss of nasal cartilage. The cartilage loss is either surgically replaced with autologous cartilage or synthetic grafts. However, these replacement options come with donor-site morbidity and resorption issues. 3-dimensional (3D) bioprinting technology offers the opportunity to engineer anatomical-shaped autologous nasal cartilage grafts. The 3D bioprinted cartilage grafts need to embody a mechanically competent extracellular matrix (ECM) to allow for surgical suturing and resistance to contraction during scar tissue formation. We investigated the effect of culture period on ECM formation and mechanical properties of 3D bioprinted constructs of human nasal chondrocytes (hNC)-laden type I collagen hydrogel in vitro and in vivo. Tissue-engineered nasal cartilage constructs developed from hNC culture in clinically approved collagen type I and type III semi-permeable membrane scaffold served as control. The resulting 3D bioprinted engineered nasal cartilage constructs were comparable or better than the controls both in vitro and in vivo. This study demonstrates that 3D bioprinted constructs of engineered nasal cartilage are feasible options in nasal cartilage reconstructive surgeries.

## Keywords

Skin cancer, nasal cartilage, septal chondrocytes, tissue engineering, hydrogel, bioprinting, nude mice

Date received: 27 November 2021; accepted: 23 February 2022

## Introduction

Non-melanoma skin cancers (NMSCs), including basal cell carcinoma (BCC) and squamous cell carcinoma (SCC), are the most frequent malignant skin cancers in the Caucasian population.<sup>1,2</sup> Since 1960, it has been reported that there has been a 3% to 8% yearly increase in the incidence of NMSCs worldwide.<sup>1</sup> In the USA, it's estimated that the incidence of NMSCs is more than 1,000,000 cases per year.<sup>1</sup> Among the NMSCs cases, roughly 36% include the nasal alar lobule, which accounts for the highest regional frequency.<sup>3</sup> Therefore, it is not uncommon for the fibromuscular tissue around the alar lobule and nasal septal cartilage to be removed during tumor resection to establish clear margins.<sup>3</sup> After the tumor resection, nasal reconstructive surgery is usually necessary for restoring structural support and facial esthetic.<sup>3–6</sup> In particular, the

<sup>1</sup>Department of Civil and Environmental Engineering, Faculty of Engineering, University of Alberta, Edmonton, AB, Canada

<sup>2</sup>Division of Orthopedic Surgery and Surgical Research, Department of Surgery, University of Alberta, Edmonton, AB, Canada

<sup>3</sup>Institute for Reconstructive Sciences in Medicine, Misericordia Community Hospital, Edmonton, AB, Canada

<sup>4</sup>Division of Otolaryngology, Department of Surgery, University of Alberta, Edmonton, AB, Canada

### Corresponding authors:

Yaman Boluk, Department of Civil and Environmental Engineering, University of Alberta, 7-273 Donadeo Innovation Centre for Engineering, Edmonton, AB T6G 2H9, Canada.  
Email: yaman.boluk@ualberta.ca

Adetola B Adesida, Department of Surgery, Faculty of Medicine & Dentistry, University of Alberta, 3.002E Li Ka Shing Centre for Health Research Innovation, Edmonton, AB T6G 2E1, Canada.  
Email: adesida@ualberta.ca



critical structural support restoration step during nasal reconstruction is currently achieved by inserting an allogeneic, synthetic, or autologous cartilage graft.<sup>3</sup> Despite being clinically used, these materials have shown drawbacks that are yet to be resolved.

Allogeneic grafts are decellularized specimens that have been harvested from live or cadaveric donors. These grafts appear attractive since they are biocompatible and theoretically non-immunogenic.<sup>7</sup> However, the main drawback of allogeneic grafts is their high resorption rates. It was found that allogeneic costal cartilage grafts experienced a resorption rate of 31%<sup>8</sup> compared to 3% in the autologous tissue.<sup>9</sup> Synthetic grafts have also been explored due to their low immunogenicity and lack of donor-site morbidity. Materials that commonly have been used include silicon, porous high-density polyethylene (MedPor), or expanded polytetrafluoroethylene (Gore-tex).<sup>10</sup> The drawbacks of synthetic materials, however, include infection, resorption, dislocation, and extrusion. For instance, the infection rate that has been associated with silicone, MedPor, and Gore-tex grafts are 3.9%, 20%, 5.3% respectively.<sup>10</sup> Autologous grafts are currently the golden standard used in nasal reconstructive surgery due to the absence of immunogenicity.<sup>3</sup> However, due to a lack of septal cartilage, sourcing cartilage from other body parts such as the ear and ribs, is common. Extracting cartilage from other areas presents the issue of donor-site morbidity. Also, some extracted tissues are considered to have inferior handling qualities and present the issue of warping (such as with costal cartilage).<sup>11</sup>

More recently, cell-based engineered cartilage grafts have shown the potential to overcome these drawbacks associated with the use of conventional cartilage grafts.<sup>3,12</sup> Previous studies have shown that dedifferentiated hNCs are a promising cell source with a redifferentiation capacity to generate hyaline-like cartilages.<sup>3,13–17</sup> A large number of autologous hNCs can be generated from a small cartilage biopsy taken from the nasal septum by expanding the cells in the presence of specific growth factors and autologous serum.<sup>3,12</sup> Together with appropriate biomaterials, biochemical factors, and mechanical stimuli, it is possible to achieve cellular differentiation and thus, cartilage graft generation that can be subsequently implanted without an immune reaction.<sup>3,12</sup> The first human trial implementations of engineered cartilage from hNCs using the clinically approved collagen scaffold, Chondro-Gide, have already been successfully demonstrated.<sup>3</sup> However, despite these early successes, there are still some prominent drawbacks associated with the use of engineered constructs, such as the limited shapes of commercially available scaffolds and the inhomogeneous distribution of hNCs during manual dispersion of hNCs.

Three-dimensional (3D) bioprinting approaches allow a rapid additive fabrication of patient specific, anatomically, or surgical ready shaped engineered functional tissue by

cooperate tissue engineering technique.<sup>18,19</sup> Through computer aided design (CAD) tools, the 3D bioprinting process enables the precise dispensation of the hydrogels and living cells (known as bioink) from a movable printing head into a biomimetic scaffold with homogeneous cell distribution.<sup>20,21</sup> Bioink can be considered one of the most important aspects of the bioprinting process since an ideal bioink should satisfy both cell compatibility for tissue regeneration and printability to support the printing process. In 3D bioprinting of nasal cartilage, bioinks that are successfully used in 3D bioprinting application include natural polymers such as collagen,<sup>22</sup> gelatin,<sup>23</sup> alginate,<sup>24</sup> cellulose,<sup>25–28</sup> agarose.<sup>29</sup>

To this date, the results from recent research did not provide enough *in vivo* evidence that customized 3D bioprinted engineered nasal cartilage could achieve similar clinical promises to that of the commercial Chondro-Gide scaffold.<sup>16,26,27</sup> In the work of Yi et al.,<sup>16</sup> a 3D-printed PCL scaffold using human adipose stem cell-laden cartilage-derived hydrogels, was implanted subcutaneously in a nude mice model. Unfortunately, the *in vivo* stability of the constructs, including calcification, vascularization, and bone formation, were not studied. Gatenholm's group utilized cellulose-based hydrogels with hNCs to bioprint neo-cartilages which were implanted in a mice model.<sup>26,27,30</sup> Yet, the quantitative biochemical and biomechanical data, and *in vivo* stability were not reported in this study.

In our previous study, we successfully generated engineered nasal septal cartilage using type I collagen hydrogel via the freeform reversible embedding of suspended hydrogels (FRESH) bioprinting method, where the *in vitro* biochemical results highly resembled that of native tissue.<sup>22</sup> To further support its potential for clinical application and formation of patient-specific surgical—ready shapes, the mechanical characterization, and *in vivo* stability of the engineered nasal cartilage substitutes is needed. Herein, we first demonstrated the ability to 3D bioprint patient-specific lower lateral cartilage from Computed tomography (CT) scans. We then investigated the effects of chondrogenic culture on the biochemical and mechanical properties of bioprinted constructs of hNCs *in vitro* and *in vivo* in nude mice. Engineered nasal cartilage from hNCs seeded on clinically approved type I and II collagen membrane scaffolds (Chondro-Gide) served as a control.

## Materials and methods

### Ethics

Human nasal septal cartilage specimens were collected from surgical discards of patients undergoing nasal reconstructive surgeries with the approval of the University of Alberta's health research ethics board—biomedical panel (Study ID: Pro00018778). The animal research work was conducted and approved in accordance with the protocol

**Table 1.** Donors information.

Donor	Biological sex	Age	Medical history	In vivo implantation
1	Male	21	Asthma	Yes
2	Male	25	Deviated septum	No
3	Male	30	N/A	Yes
4	Male	30	Deviated septum	no
5	male	43	Deviated septum	No
6	Male	48	N/A	Yes

approved by the University of Alberta Animal Care User Committee (Study ID: AUP00001363).

### Human nasal chondrocyte isolation

Human nasal septal cartilage specimens were collected from six male donors undergoing septoplasty or rhinoplasty. Donors ranged from 21 to 48 years old with a mean  $\pm$  standard deviation (SD) of  $32.83 \pm 10.49$  years (refer to Table 1 for donor information). The isolation and expansion of hNCs were performed as previously described.<sup>31</sup> In brief, nasal cartilage specimens were digested with 0.15% (w/v) collagenase II solution (300 units/mg) for 22 h at 37°C in an incubating shaker. hNCs were then harvested and plated at a density of 104 cells/cm<sup>2</sup> and cultured in a standard medium: Dulbecco's Modified Eagle Medium (DMEM) supplemented with 10% (v/v) FBS, 1 ng/ml of transforming growth factor beta 1 (TGF- $\beta$ 1), and 5 ng/ml of fibroblast growth factor 2 (FGF-2) in a normoxic humidified incubator (21% O<sub>2</sub>, 5% CO<sub>2</sub>). The media was changed twice per week. The gross morphology of the nasal chondrocytes during the monolayer expansion are shown in Supplemental Figure S1. Passage 2 (P2) cells were used for bioprinting. The population doubling (PD) of hNCs for each donor were calculated by the equation:  $PD = \log_2(\text{population}_{\text{final}} / \text{population}_{\text{initial}})$  for each passage. The cumulative PD (CPD) is the sum of PD at passage 1 and passage 2. The CPD reflects the total number of times primary hNCs from the donors have doubled. The CPD and CPD/day for each donor is provided in Supplemental Table S1.

### Nasal chondrocyte-laden bioink preparation

hNCs were trypsinized and resuspended in a defined serum-free chondrogenic media (SFM) composed of DMEM, 100 U/ml penicillin and streptomycin with 2 mM L-glutamine (Life Technologies, all), 100 mM HEPES, insulin-transferrin-selenium (ITS) + 1, 0.1  $\mu$ M dexamethasone, 0.1 mM ascorbic acid 2-phosphate, and 0.1 mM L-proline at a concentration of  $0.875 \times 10^7$  cells/ml. The cell suspension was diluted in a 1:10 ratio with type I collagen gel (3.5 wt%, Lifeink 200, Advanced Biomatrix, LOT: 5202-1KIT, USA) to create a final concentration of

$8.75 \times 10^6$  cells/ml. The resulting cell-laden bioink is a neutralized type I collagen solution that is thermoresponsive and can polymerize at 37°C.

### 3D bioprinting of type I collagen hydrogels and cell seeding of Chondro-Gide scaffolds

The bioink is then used to fabricate patient-specific lower lateral nasal cartilage shapes, using a micro-extrusion base bioprinter INKREDIBLE+ (CELLINK, Sweden). The sterile gelatin support bath (LifeSupport, Advanced Biomatrix, USA) was prepared according to the manufacturer's instructions. The filaments and the microstructures of the printed constructs were pre-defined in a 3D bioprinting software (Slic3r, USA). A CT-scanned patient-specific right lower lateral nasal cartilage with 90% infill rate, was first bioprinted inside support bath using type I collagen bioink, to show the printability of autologous cartilage. In order to compare the mechanical and in vivo behaviors of the bioprinted constructs with the cell-seeded clinically approved Chondro-Gide scaffolds, the collagen bioink was the bioprinted into a strip shape with a dimension of 25 mm length  $\times$  6 mm width  $\times$  2 mm height (same dimensions as Chondro-Gide). These 3D bioprinted cell-laden strip shaped constructs were then cultured in serum-free chondrogenic medium (4 ml per construct and changed twice per week) in normoxia for 3, 6, 9 weeks.

Clinically approved type I/III collagen membrane scaffolds (Chondro-Gide, Geistlich Pharma, Wolhusen, Switzerland) served as the control group. Chondro-Gide scaffolds (25 mm (length)  $\times$  6 mm (width)  $\times$  2 mm (thickness)) were cut with scalpels from the same lot to control the lot-to-lot variability. 2.625 million hNCs were seeded onto the porous side of the scaffolds (same cell number as bioprinted scaffold) and then cultured in 4 ml of defined serum-free chondrogenic medium with TGF- $\beta$ 3. The schematic experimental setup is shown in Figure 1.

### Culture condition

**In vitro culture condition.** Both 3D bioprinted type I collagen hydrogel constructs and Chondro-Gide scaffolds (control group) were cultured in normoxic humidified incubators. Media changes were performed twice a week. To provide sufficient time for the constructs and scaffolds to develop mechanical strength before in vivo culture, three culture periods were first evaluated, including 3, 6, 9 weeks. Only the constructs and scaffolds cultured from one of the selected periods, which showed best mechanical strength and chondrogenic phenotype, were then subjected to further in vivo study.

**In vivo culture condition.** To study the in vivo behavior of engineered nasal cartilage, the in vitro cultured bioprinted type I collagen hydrogel constructs and Chondro-Gide

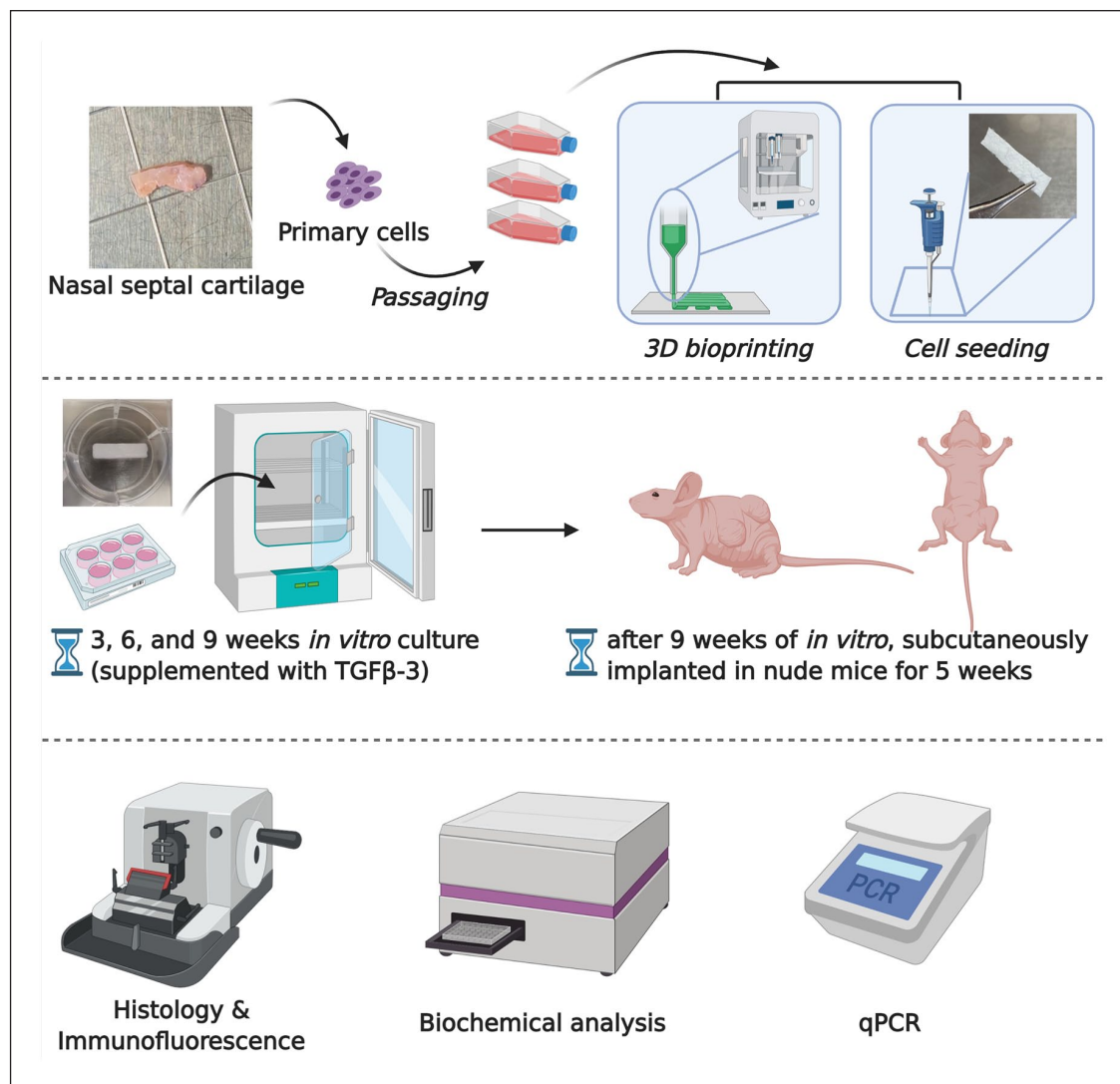


**Figure 1.** Schematic diagram of experimental design.

scaffolds were divided into two experimental groups ( $n=3$ , three donors). Experimental group I involved five additional weeks of *in vivo* culture after being implanted subcutaneously in nude mice, whereas experimental group II involved five additional weeks of *in vitro* culture in chondrogenic media to serve as a comparison group.

For experimental group I, the *in vitro* cultured constructs and scaffold was first cut into smaller sizes to reduce the size of the implants. Then *in vitro* cultured constructs and scaffolds were implanted into the back of athymic CD-1 nude mice ( $n=7$ , seven mice, 6-week-old, Charles River, Wilmington, USA) as previously described.<sup>13</sup> Each mouse received a pair of *in vitro* cultured bioprinted construct and Chondro-Gide scaffold, and the engineered cartilage from same experimental group were implanted in different mice. Six nude mice were implanted with the engineered nasal cartilages, with a total of six bioprinted constructs and six Chondro-Gide

scaffolds. One additional mouse served as a control and received empty scaffolds (cultured bioprinted construct and Chondro-Gide scaffold without cells). Two small caudal subcutaneous incisions (4–5 mm) were dissected on the skin of each mouse. The constructs and scaffolds were then implanted in the subcutaneous pockets. Incisions were closed with suture and cyanoacrylate tissue adhesive. No post-surgical complications were observed. Five weeks following the implantation, the mice were euthanized by CO<sub>2</sub> inhalation, and the constructs and scaffolds were macroscopically dissected from the murine subcutaneous tissues. Gross morphology pictures were taken before and after implantation.

#### Live/dead assay

Cell viability analysis was conducted using a live/dead viability kit (ThermoFisher, USA). The *in vitro* cultured

constructs and scaffolds from three donors (at day 0, 3 weeks, 6–9 weeks of culture) were incubated in 1 ml of 4  $\mu$ M calcein AM and 1 ml of 2  $\mu$ M ethidium homodimer-1 solution at room temperature in the dark for 30 min. They were then examined under a Nikon con-focal laser scanning microscope (Leica TCS SP5, German). The cell viability was quantified using Fuji Image J software.

### Evaluation of cartilage formation

**Sulfated glycosaminoglycans per DNA quantification.** To measure the glycosaminoglycan (GAG) matrix content and the DNA content of the in vitro cultured engineered cartilages, the bioprinted constructs and Chondro-Gide scaffolds were weighed, cut into smaller pieces, and rinsed twice with Phosphate Buffered Saline (PBS), and then frozen at  $-80^{\circ}\text{C}$ . They were then thawed and digested in Proteinase K solution (1 mg/ml) at  $56^{\circ}\text{C}$  overnight for 16 h.

The GAG matrix content of the engineered cartilages was measured by a 1,9-dimethylmethylene blue (DMMB, Sigma Aldrich, Canada) assay with chondroitin sulfate (Sigma Aldrich, Canada) used as the internal standard.<sup>32</sup> The GAG contents were evaluated on the V-max kinetic microplate reader (Molecular Devices, USA) at a wavelength of 530 nm.

The DNA contents were measured using the CyQUANT Cell Proliferation Assay Kit (Thermo Fisher). Calf thymus DNA (Sigma) was used as the standard. Fluorescence emission was measured at 580 nm (excitation 450 nm). The DNA contents were measured on a CytoFluor II fluorescence multi-well plate reader (PerSeptive Biosystems).

The quantity of GAG was then normalized to the total DNA content and wet weight of each engineered cartilage for the six donors.

**Histology and immunofluorescence.** For both in vitro and in vivo engineered cartilages, the samples were fixed in 10% (v/v) neutral buffered formalin at  $4^{\circ}\text{C}$  overnight, dehydrated through a series of alcohol washes, and then embedded in paraffin wax. The embedded samples were sectioned into 5  $\mu$ m thick slices and deparaffinized by xylene substitute. The sliced sections were rehydrated through a graded series of ethanol (100%–96%, 70% and 50% (v/v)), and rinsed in distilled water. Then, the prepared samples were evaluated for histology staining including Safranin-O/Fast Green, Masson Trichrome, and Alizarin Red, as well as immunofluorescence stains including type I and II collagen, type  $\times$  collagen, CD31, Bone Sialoprotein (BSP), and F4/80 (BM8). Imaging was carried out using Nikon Eclipse Ti-S microscope coupled to a DS-U3/Fi2 Color CCD camera using 100x objective lenses.

For Safranin-O/Fast Green assessment, the prepared samples were stained with Meyer's Hematoxylin, Green FCF, and Safranin-O. For Masson Trichrome assessment (NovaUltra™ Masson Trichrome Stain Kit, USA), the

samples were stained with Weigert's Iron Hematoxylin, Biebrich Scarlet-Acid Fuchsin, phosphomolybdic-phosphotungstic acid, aniline blue, and acetic acid solutions. For Alizarin red assessment, the samples were immersed in 2% (w/v), pH 4.1–4.3 Alizarin red (Sigma-Aldrich, Canada) solution for 2.5 min. After each of the histology staining, the stained slides were rinsed with distilled water and then dehydrated again with ethanol (95% (v/v) and 100%). The slides were mounted with mounting media (Richard-Allan Scientific, Thermo Scientific) to prepare for imaging.

Type I and II collagen protein expressions were examined by immunofluorescence. After antigen retrieval, slides were incubated with rabbit anti-collagen I (CL50111AP-1, Cedarlane, Canada) and mouse anti-type II collagen, both primary antibodies are diluted in 1:200 ratio (II-II6B3, Developmental Studies Hydromat Band, USA) overnight to allow for type I and II collagen bindings, respectively. Secondary antibodies (goat anti-rabbit IgG Alexa Fluor 594, ab150080; goat anti-mouse IgG Alexa Fluor 488, ab150117; Abcam, USA) were incubated with the slides for 45 min, both secondary antibodies are diluted in 1:200 ratio. Sectioned slides were additionally stained with 4',6-diamidino-2p-phenylindole (DAPI, ThermoFisher, USA) for 20 min at room temperature to observe the nuclei of hNCs within each sample. Sections were mounted with 1:1 Glycerol:PBS to prepare for imaging. The same DAPI staining and mounting methods applies to all immunofluorescence staining preparations.

The protein expression of type  $\times$  collagen was also examined by immunofluorescence. Slides were incubated overnight with rabbit anti-type  $\times$  collagen antibodies in 1:100 dilution ratio (rabbit polyclonal to type  $\times$  collagen, ab58632, Abcam, USA) to bind type  $\times$  collagen and subsequently labeled by secondary antibody (goat anti-rabbit IgG Alexa Fluor 594, ab150080, Abcam, USA).

Immunofluorescence imaging was also used to assess the vascular invasion protein, CD31. For CD31, the primary antibody used was anti-mouse CD31 (CD31/PECAM Biotinylated Antibody, BAF3628, R&D systems, USA) in 1:100 dilution ratio, then Alexa Fluor 488 conjugated streptavidin in 1:100 dilution ratio (S32354, Life Technology, USA) was used to label the biotinylated primary antibody.

Immunofluorescence was further used to examine the bone associated protein, bone sialoprotein (BSP). The primary antibody was anti-bone sialoprotein, diluted in 1:100 ratio (ab195426, Abcam, USA), and was labeled by secondary antibody, goat anti-rabbit IgG Alexa Fluor 594 (ab150080, Abcam, USA) in 1:200 dilution ratio.

The F4/80 (BM8) molecule, solely expressed on the surface of macrophages, was examined by immunofluorescence. Following antigen retrieval described by Lee et al.,<sup>33</sup> slides were incubated with Biotinylated F4/80 (BM8) primary antibody (13-4801-82, ThermoFisher

**Table 2.** Primer Sequences for Real-Time RT-qPCR.

Genes	Forward Primer (5')	Reverse Primer (3')
Beta-actin ( <i>ACTB</i> )	AAGCCACCCCACTTCTCTCTAA	AATGCTATCACCTCCCCTGTGT
Beta-2 microglobulin ( <i>B2M</i> )	TGCTGTCTCCATGTTTGATGTATCT	TCTCTGCTCCCCACCTCTAAGT
Tyrosine 3-mono-oxygenase/ Tryptophan 5-monooxygenase activation protein zeta ( <i>YWHAZ</i> )	TCTGTCTTGTACCAACCATTCTT	TCATGCGGCCTTTTTTCCA
Aggrecan ( <i>ACAN</i> )	AGGGCGAGTGGAATGATGTT	GGTGGCTGTGCCCTTTTTTAC
Collagen I ( <i>COL1A2</i> )	GCTACCCAACCTTGCCCTTCATG	GCAGTGGTAGGTGATGTTCTGAGA
Collagen II ( <i>COL2A1</i> )	CTGCAAATAAAATCTCGGTGTTCT	GGGCATTTGACTCACACCAGT
SRY-Box 9 ( <i>SOX9</i> )	CTTTGGTTTGTGTTTCGTGTTTTG	AGAGAAAAGAAAAGGGAAAGGTAAGTTT
Collagen X ( <i>COL10A1</i> )	GAAGTTATAATTTACTGAGGGTTTCAA	GAGGCACAGCTTAAAAGTTTAAACA
Runt related transcription factor 2 ( <i>RUNX2</i> )	GGAGTGGACGAGGCAAGAGTTT	AGCTTCTGTCTGTGCCTTCTGG
Peroxisome proliferative activated receptor gamma ( <i>PPAR<math>\gamma</math></i> )	AAGCTGCTCCAGAAAATGACAGA	CGTCTTCTTGATCACCTGCAGTA
Lysyl oxidase like 2 ( <i>LOXL2</i> )	ACGGCCACCGCATCTG	TCCGTCTCTTCGCTGAAGGA

Scientific, Canada) in 1:100 dilution ratio. Slides were then incubated with streptavidin in 1:100 dilution ratio (S32354, Life Technology, USA), Alexa Fluor 488 conjugate in 1:200 dilution ratio (S32354, Life Technology, USA) prior to imaging.

**Real-time RT-qPCR.** RT-qPCR was used to measure relative gene expression of chondrogenic (e.g. *ACAN*, *COL2A1*, *SOX9*), fibrogenic (e.g. *COL1A2*), hypertrophic (e.g. *COL10A1*, *RUNX2*), and angiogenic markers (e.g. *PPAR $\gamma$* ), of hNCs after 3, 6, 9 weeks of culture. Expression of the collagen cross linking enzyme (*LOX*) was also analyzed by RT-qPCR at each of the culture times. Total RNA was extracted with Trizol reagent (Life Technologies) according to the manufacture instructions. RNA was immediately transferred to Trizol upon harvesting to prevent changes in gene expression. The purity and concentration of isolated RNA were examined with Nanodrop One C. One hundred nanogram total RNA was reverse transcribed to cDNA by GoScript reverse transcriptase (Promega Corporation, WI, USA.) with 1  $\mu$ g of oligo (Dt) primers (Promega Corporation, WI, USA). RT-qPCR was performed as we have previously described<sup>34</sup> (primers sequences are presented in Table 2). The mRNA expression levels for each primer set were normalized to the housekeeping genes,  $\beta$ -actin (*ACTB*), Beta-2 microglobulin (*B2M*), and Tyrosine 3-Monooxygenase/Tryptophan 5-Monooxygenase Activation Protein Zeta (*YWHAZ*), using the  $2^{-\Delta C_t}$  method.

### Mechanical properties of cell seeded Chondro-Gide scaffolds and bioprinted constructs

After 3, 6, 9 weeks of chondrogenic culture, simple interrupted suture tests were performed for both type of engineered cartilages at each time point. Briefly, to test the

durability of the cartilages, a single 5-0 PROLENE suture was introduced through each engineered cartilage and a knot was tied. Subsequent knots were then made if the cartilages were strong enough.

Three-point bending results were measured by Dynamic Mechanical Analysis Q800 (TA instrument, USA). Small 5 mm three-point bending clamps were used for the test. Engineered cartilage tissues were placed on top of the 5 mm stationary clamp, and a movable clamp moving 0.1 N/s was used to measure the force responses.

### Microstructure of cell seeded Chondro-Gide scaffolds and bioprinted constructs

The ultrastructure of the 3D bioprinted constructs and Chondro-Gide scaffolds at each in vitro culture period (3, 6, 9 weeks) were investigated by scanning electron microscopy (SEM, Hitachi, JA, Model S-4800). All reagents and accessories used were from Electron Microscope Science, PA, USA. Each construct and scaffold were fixed with 2% (v/v) glutaraldehyde and 2.5% (v/v) paraformaldehyde in sodium cacodylate trihydrate buffer at 4°C overnight. Constructs and scaffolds were then cut in half using scalpels and washed with Milli-Q water twice for 2 min each the next day. The constructs and scaffolds were then post fixed in 2% (w/v) osmium tetroxide ( $\text{OsO}_4$ ) and 2% (w/v) tannic acid. Post fixing and dehydration steps were as we have previously described.<sup>31</sup> The images of the engineered cartilages were captured using SEM (Zeiss Sigma 300 VP-FESEM).

### Semi-quantitative Analysis

Safranin-O staining of in vitro engineering cartilages is evaluated using the Bern score semi-quantitative method,

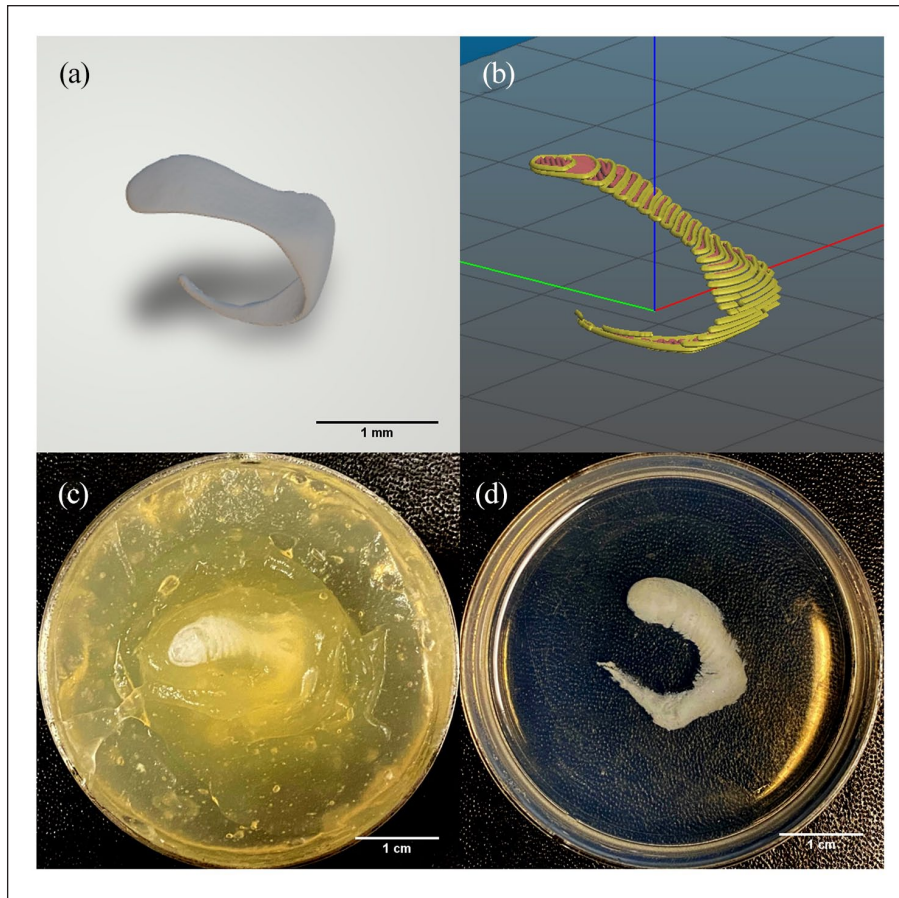


**Figure 2.** Gross morphology of the FRESH printed structure. (a) 3D model of a right lower lateral nasal cartilage from CT imaging and (b) the preview of the sliced nasal cartilage using Slic3r software. (c) 3D bioprinted lower lateral nasal cartilage in gelatin support bath before and (d) after 30 min incubation in 37°C. Following the 30-min incubation, the support bath was aspirated, and PBS was added.

which accounts for uniformity and darkness of the staining, the distance between cell and matrix, as well as cell morphology. In this study, the Bern scores are evaluated by four blinded observers.<sup>35</sup> The immunofluorescence staining of Type I and II collagens is semi-quantified using python. The immunofluorescence intensities are normalized by cell number (DAPI).

#### Data analysis and statistical methods

For biochemistry, gene expression, and mechanical test analysis, a repeated measures two-way analysis of variance (RM-ANOVA) test was used to assess for interaction between culture time and scaffold type. Culture time and scaffold type were treated as within-subject factors, the donors were treated as repeated measurements. If the interaction was non-significant, the main effects of culture time and scaffold type were reported. If the interaction was significant, the  $p$ -value was reported. Bonferroni post hoc tests were performed for the pairwise comparisons to compare within culture time and scaffold type. Cell viability

was analyzed by pairwise comparisons between day 1 and 3, 3, 6, 6, 9 weeks. Data are presented as mean  $\pm$  SD. All analyses were performed using GraphPad Prism 8. A  $p$ -value of  $p < 0.05$  was considered statistically significant. A  $p$ -value between 0.05 and 0.1 was considered borderline significant.

## Results

### 3D bioprinting of engineered cartilage with autologous shapes

A patient-specific right lower lateral nasal cartilage was bioprinted using the FRESH method to demonstrate the ability of fabricating autologous shaped cartilages. Figure 2(a) shows the STL image generated from CT, and the internal structure of the bioprinted cartilage in Figure 2(b). Figure 2(c) and (d) show the 3D bioprinted nasal cartilage before and after the gelatin support bath melted, respectively. As temperature increased to 37°C, the construct printed in the FRESH support bath started to dissolve and

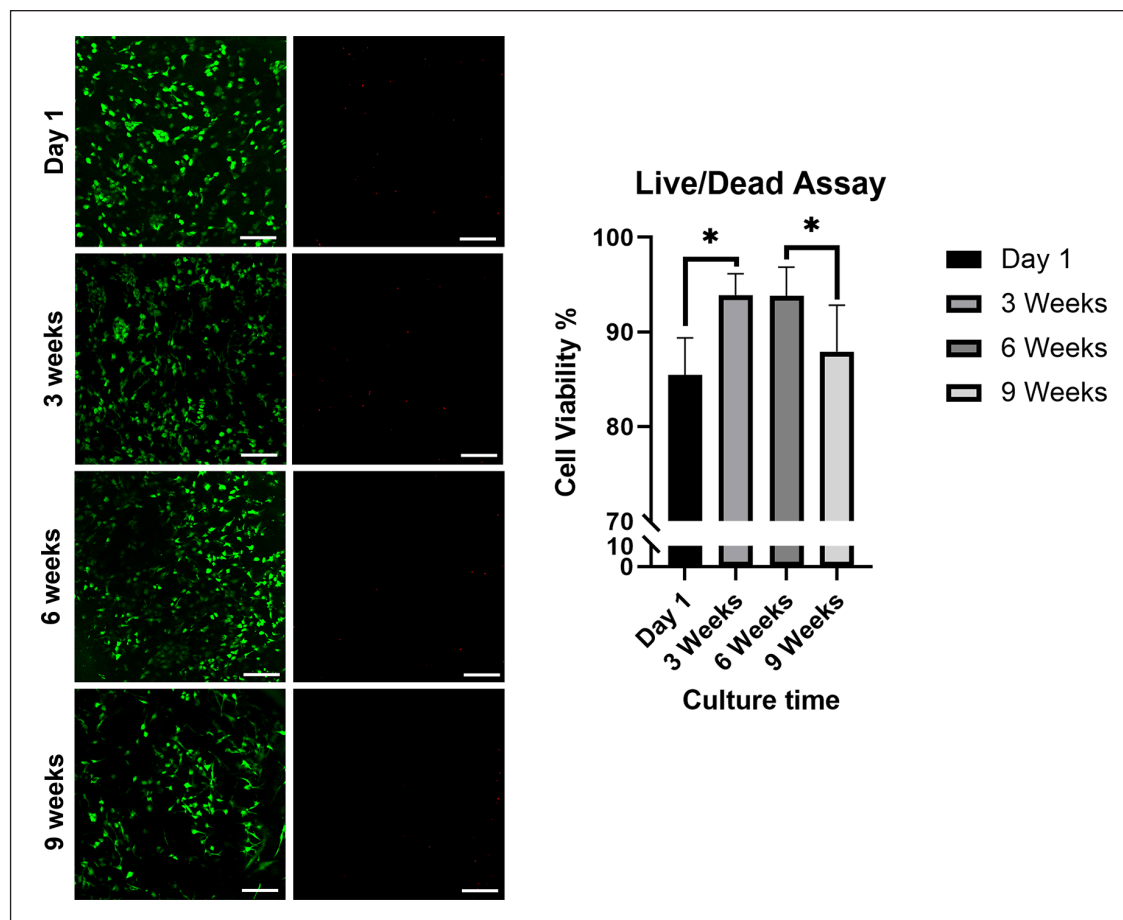


**Figure 3.** (a) Live/dead assay (b) cell viability over culture time. Paired *t*-tests were done to compare cell viability between day 1 versus 3, 3 versus 6 weeks, and 6 versus 9 weeks. \*Represents  $0.01 < p < 0.05$ . Scale bar: 100  $\mu$ m.

caused the bioprinted collagen bioink to self-assemble and form a hydrogel to maintain its structural integrity.

#### Live/dead analysis of bioprinted constructs

A Live/Dead fluorescent assay was used to assess the cell viability of the constructs following 3D bioprinting. The cell viability of constructs cultivated for 1 day, 3, 6, 9 weeks were  $85.5 \pm 3.9$ ,  $93.9 \pm 2.3$ ,  $93.8 \pm 3.1$ ,  $87.9 \pm 4.9$ , respectively (Figure 3). Paired *t*-tests for the interested groups were conducted between day 1 and 3, 3, 6, 6, 9 weeks. There was no significant difference in cell viability between 3 and 6 weeks of culture ( $p=0.9765$ ). Between 1 day and 3 weeks ( $p=0.0133$ ), and 6–9 weeks ( $p=0.0370$ ), a significant increase and decrease in cell viability was observed, respectively.

#### Histological analysis of in vitro engineered cartilages

After 3, 6, 9 weeks of chondrogenic culture, bioprinted, Chondro-Gide, and non-cellular cartilages, were processed,

embedded in paraffin, cut, and then stained with Safranin-O/Fast Green staining and Masson Trichrome staining. Safranin-O was used to stain sulfated proteoglycans while Fast Green served as a counter stain for protein.<sup>36</sup> Weigert's Hematoxylin, Aniline blue, and Biebrich scarlet-acid fuchsin of the Masson Trichrome stain, were used to stain for nuclei, collagen, and cytoplasm/keratin, respectively.<sup>37</sup> Empty scaffolds did not show evidence of matrix synthesis, denoted by the absence of positive Safranin-O staining for proteoglycans. Only background staining for Fast Green was present in empty scaffolds. Chondro-Gide scaffolds were shown to have two different layers following Safranin-O/Fast Green staining, corresponding to the compact and porous layers. The porous layer was the cell seeding side. At 3 weeks of culture, both bioprinted constructs and Chondro-Gide scaffolds showed proteoglycan rich matrix deposition denoted by positive Safranin-O staining (Figure 4(a)). As culture time increased from 3 to 9 weeks, the intensity of Safranin-O staining increased in both engineered cartilages (Figure 4(a), Safranin-O for all donors after 3, 6, 9 weeks culture are shown in Supplemental Figures S2–S4, respectively).



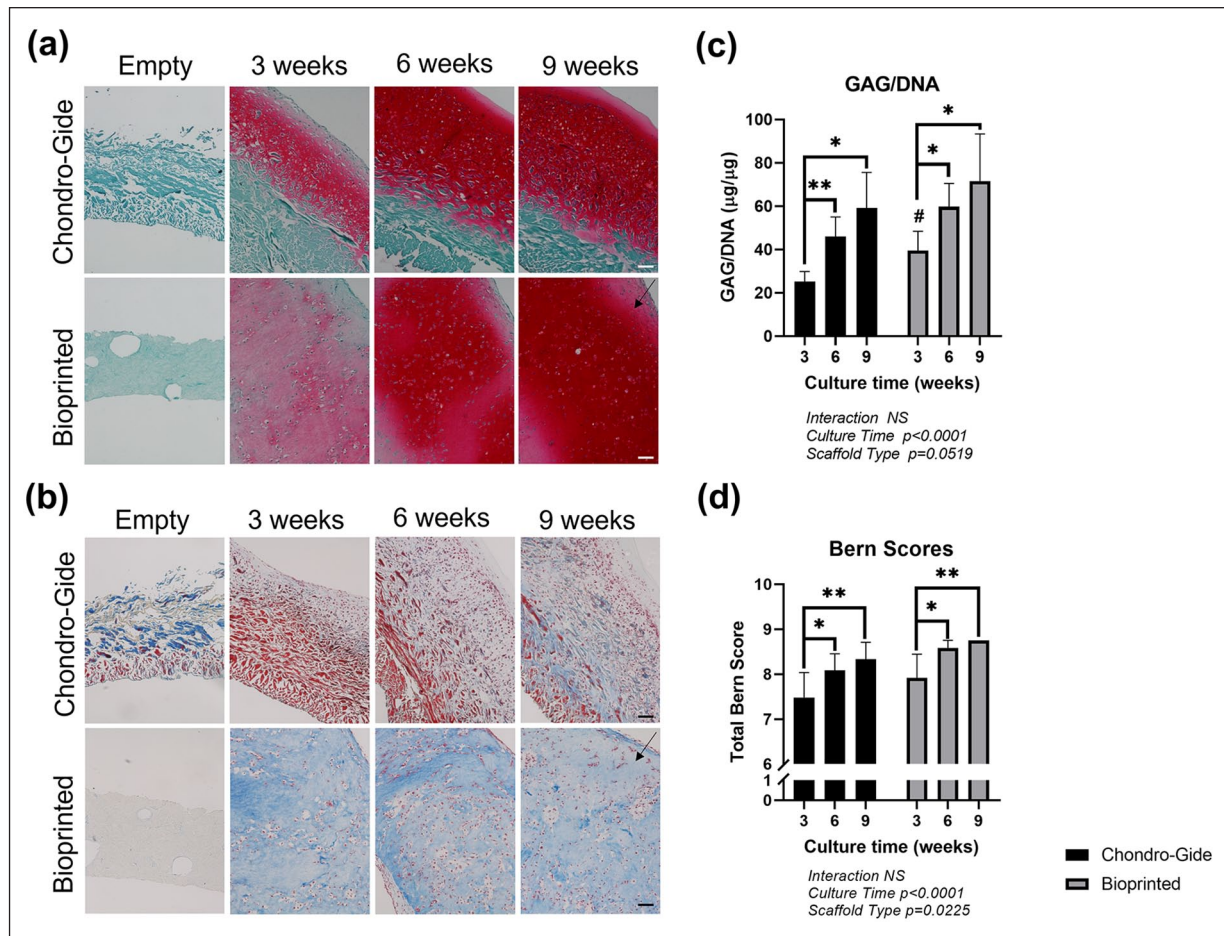


**Figure 4.** Histological and biochemical analysis of in vitro constructs across culture time. (a) Safranin-O/Fast green Staining, (b) Masson's Trichrome staining, (c) GAG/DNA of in vitro constructs and (d) Bern Score of Safranin-O staining. Black arrows indicate tissue areas that have (a) positive Safranin-O staining for aggrecan or (b) positive aniline blue for collagen (b). Data were analyzed by two-way ANOVA and corrected with the Bonferroni post hoc test. GAG: glycosaminoglycan; NS: non-significant; WW: wet weight. Scale bar: 100  $\mu$ m. Star (\*) represent the significant difference with regarding of culture time after Bonferroni post hoc correction: \* represents  $0.01 < p < 0.05$ , \*\* represents  $0.001 < p < 0.01$ . Pound (#) represent the significant difference with regarding of scaffold type after Bonferroni post hoc correction: # represents  $0.01 < p < 0.05$ .

For the Masson Trichrome staining, the empty bioprinted constructs showed only faint blue staining for collagen. Chondro-Gide empty scaffolds, however, showed both Aniline blue and Scarlet red staining corresponding to collagen and cytoplasm/keratin, respectively. The layers staining red and blue were the compact and cell seeding layers, respectively. Collagen deposition was consistent with Safranin-O staining and appeared at 3 weeks in both engineered cartilages (Figure 4(b)). The enhanced red staining and size of the Chondro-Gide scaffolds at 3 weeks, compared to the empty scaffold, was likely due to swelling of the scaffolds due to proteoglycan deposition. Bioprinted constructs overall, showed a more homogeneous distribution of ECM throughout the structure than Chondro-Gide. Since cells were only seeded on the porous surface of each Chondro-Gide scaffold, matrix deposition was limited to the porous surface. To characterize the collagen distribution, immunofluorescence for

type I and II collagen was performed. Type I and II collagens were observed in both bioprinted constructs and Chondro-Gide scaffolds across the three culture times (Figure 5(a) and Supplemental Figure S6a). Type II collagen was predominantly expressed in both engineered cartilages and was more homogeneous in bioprinted constructs. The intensity of type II collagen expression became more pronounced as culture time increased, which was consistent with Safranin-O staining (Supplemental Figure S6b). The distribution of type II collagen expression was also like Safranin-O positive matrix formation in both the bioprinted constructs and Chondro-Gide scaffolds. Additionally, to assess for the presence of a bone forming phenotype, hypertrophic collagen marker, type X collagen, immunofluorescence was performed. Type X collagen was observed in both bioprinted constructs and Chondro-Gide scaffolds across the three culture times (Figure 5(b) and Supplemental Figure S6a). Similarly, to type II collagen, the

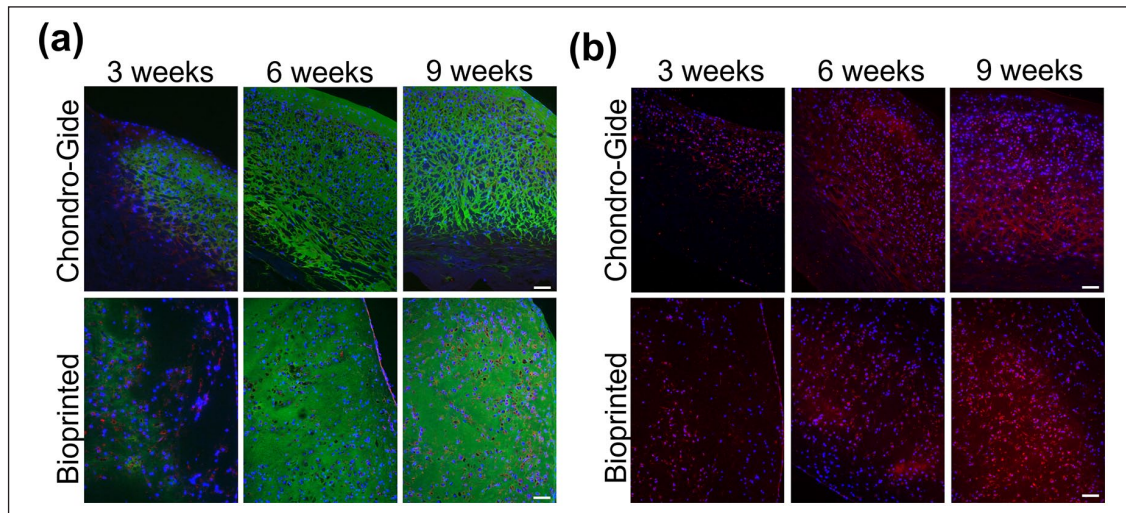


**Figure 5.** Immunofluorescence of in vitro constructs across culture time. (a) Type I (red) and II (green) collagen and (b) Type X collagen (red). The blue color is from DAPI staining, which indicate cell nuclei. Scale bar: 100  $\mu\text{m}$ .

expression of type X collagen became more pronounced with culture time (Supplemental Figure S6b).

#### GAG/DNA quantification of in vitro engineered cartilages

Biochemical analyses were performed in duplicates to quantify the GAG and DNA contents of scaffolds following each culture period (3, 6, 9 weeks,  $n=6$ ). The GAG/DNA ratios of Chondro-Gide scaffolds at 3, 6, 9 weeks were  $25.2 \pm 4.7$ ,  $46.0 \pm 9.0$ ,  $59.2 \pm 16.4$  respectively. GAG/DNA ratios of bioprinted constructs at 3, 6, and 9 weeks were  $39.6 \pm 8.9$ ,  $59.8 \pm 10.8$ ,  $71.7 \pm 21.7$ , respectively. Within both bioprinted and Chondro-Gide groups, culture time was shown to have a significant effect on GAG/DNA content ( $p < 0.0001$ , Figure 4(c)). A significant difference in GAG/DNA ratios was observed between 3 and 6 weeks ( $p=0.0040$  for Chondro-Gide,  $p=0.0113$  for bioprinted), and 3–9 weeks ( $p=0.0120$  for Chondro-Gide,  $p=0.0168$  for bioprinted) for both scaffold types. However, there was no significant difference in GAG/DNA ratios between 6 and 9 weeks of culture ( $p=0.1863$  for Chondro-Gide,  $p=0.2718$  for bioprinted). There was a borderline significant difference in GAG/DNA content between scaffold types ( $p=0.0519$ ), with bioprinted constructs showing higher GAG/DNA ratios than Chondro-Gide scaffolds (significant higher at 3 weeks with  $p=0.0269$ ). The Bern score evaluation is well correlated with the GAG/DNA assay (Figure 4(d)).

#### Mechanical properties of in vitro engineered cartilages

To assess the suturability of bioprinted constructs and Chondro-Gide scaffolds, a suture test was performed. A

single 5-0 PROLENE suture was made on the edge of each construct and scaffold and then subsequently observed for damage. Chondro-Gide scaffolds were able to withstand suturing at all time points (Figure 6(a)). Bioprinted constructs, however, were only able to withstand suturing at 9 weeks of culture. To assess the bending modulus of the engineered cartilages, a Three-Point bending test was performed on the constructs and scaffolds at each culture time. Both bioprinted constructs and Chondro-Gide scaffolds became more robust overtime. The bending modulus of Chondro-Gide scaffolds at 3, 6, 9 weeks of culture were  $0.0675 \pm 0.00995$ ,  $0.213 \pm 0.0233$ ,  $0.287 \pm 0.0513$  MPa, respectively. For bioprinted constructs, the bending modulus was  $0.0309 \pm 0.00704$ ,  $0.177 \pm 0.0557$ ,  $0.298 \pm 0.0577$  MPa at 3, 6, 9 weeks, respectively. Bending modulus was found to increase significantly with increasing culture time for both scaffold types ( $p < 0.0001$ , Figure 6(b)). The mean difference between Chondro-Gide and bioprinted bending modulus was 0.0366 MPa at 3 weeks, 0.0360 MPa at 6 weeks, and  $-0.0114$  MPa at 9 weeks. Chondro-Gide scaffolds were almost twice that of bioprinted constructs at 3 weeks, but at 9 weeks, the bioprinted constructs showed a slightly higher bending modulus compared to Chondro-Gide. Due to non-sufficient donor numbers for bending modulus testing ( $n=3$ ), no significant differences between scaffold types were observed. Bending modulus was also shown to increase with culture time to a greater degree in bioprinted constructs than Chondro-Gide scaffolds.

#### SEM of in vitro engineered cartilages

SEM was used to visualize the ultrastructural differences between bioprinted constructs and Chondro-Gide scaffolds across the different cultivation times. At 3 weeks of culture, both bioprinted constructs and Chondro-Gide

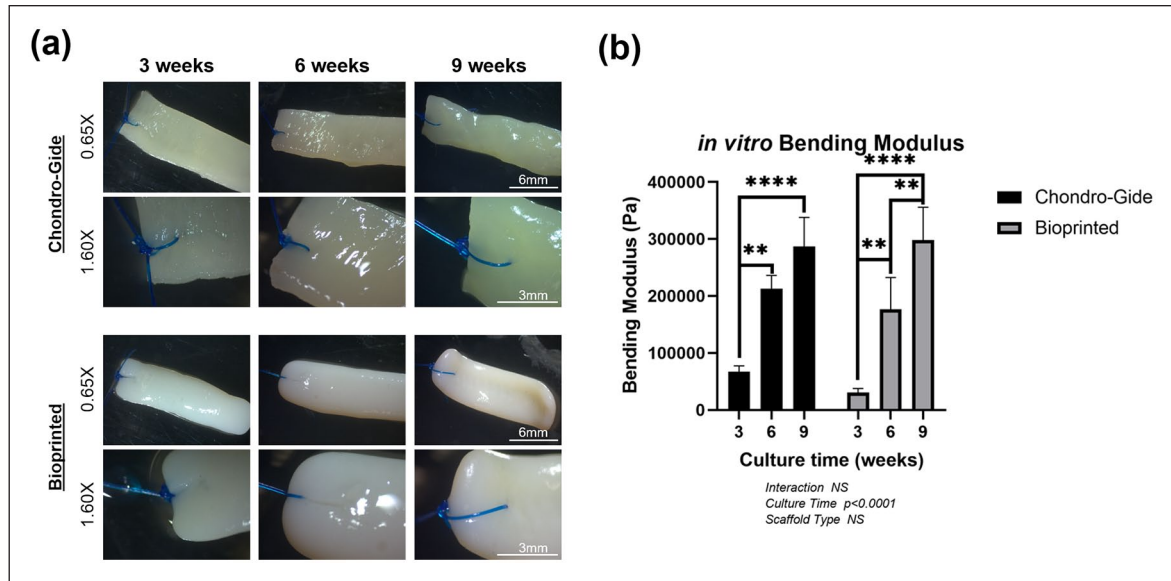


**Figure 6.** (a) Suturability of Chondro-Gide scaffolds and bioprinted constructs across culture time. Images are taken at 0.65x and 1.60x magnification. (b) Bending modulus of in vitro constructs across culture time. Data was analyzed by two-way ANOVA and corrected with the Bonferroni post hoc test. NS: non-significant. Scale bars: 6–3 mm for 0.65x and 1.60x, respectively. Star (\*) represent the significant difference with regarding of culture time after Bonferroni post hoc correction: \*\* represents  $0.001 < p < 0.01$ , \*\*\* represents  $0.0001 < p < 0.001$ , \*\*\*\* represents  $p < 0.00001$ . Pound (#) represent the significant difference with regarding of scaffold type after Bonferroni post hoc correction: # represents  $0.01 < p < 0.05$ .

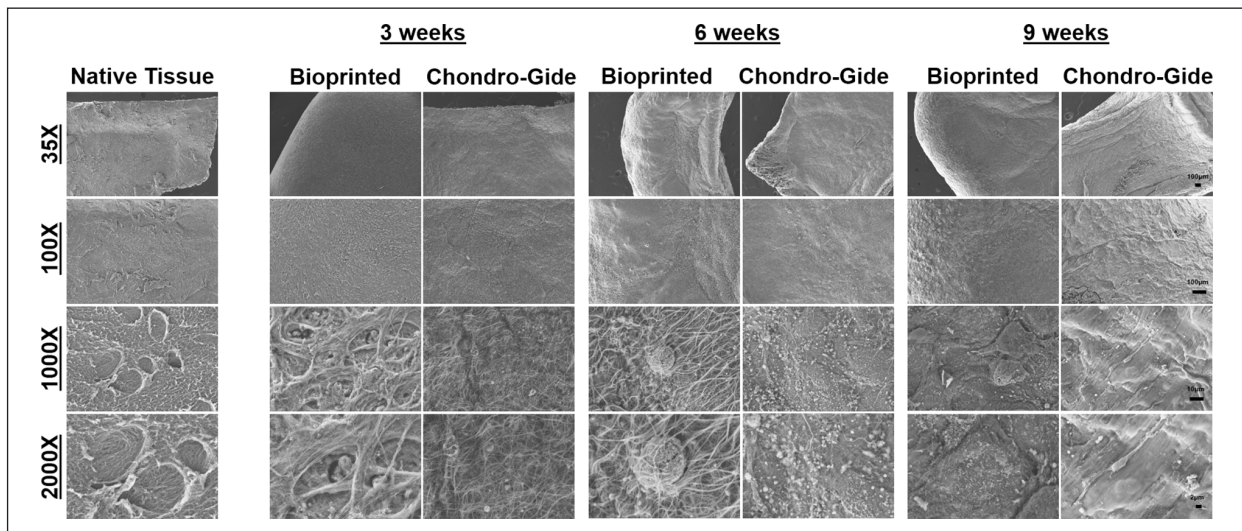


**Figure 7.** SEM imaging of in vitro constructs across culture time. Magnification of images is 35x, 100x, 1000x, and 2000x. Scale bars are 100, 10, 2  $\mu\text{m}$  for 35x/100x, 1000x, and 2000x, respectively.

scaffolds showed evidence of remodeling, denoted by the presence of fibrous structures on the surface of the cartilages (Figure 7). Chondrocytes were also found inside the lacuna structures at 3 weeks in the bioprinted constructs. After 6 weeks of culture, the distribution of ECM fibers increased and became more even in both bioprinted constructs and Chondro-Gide scaffolds, and by 9 weeks, both engineered cartilages were completely covered by a uniform layer of ECM. Bioprinted constructs at 3 weeks were

shown to resemble native tissue most closely. This resemblance however was lost at 6 weeks as more ECM was deposited on the surface of the structures.

#### Gene expression of in vitro engineered cartilages

RT-qPCR was used to quantify the expression of chondrogenic (*ACAN*, *SOX9*, *COL2A1*, *CO1A2*), hypertrophic

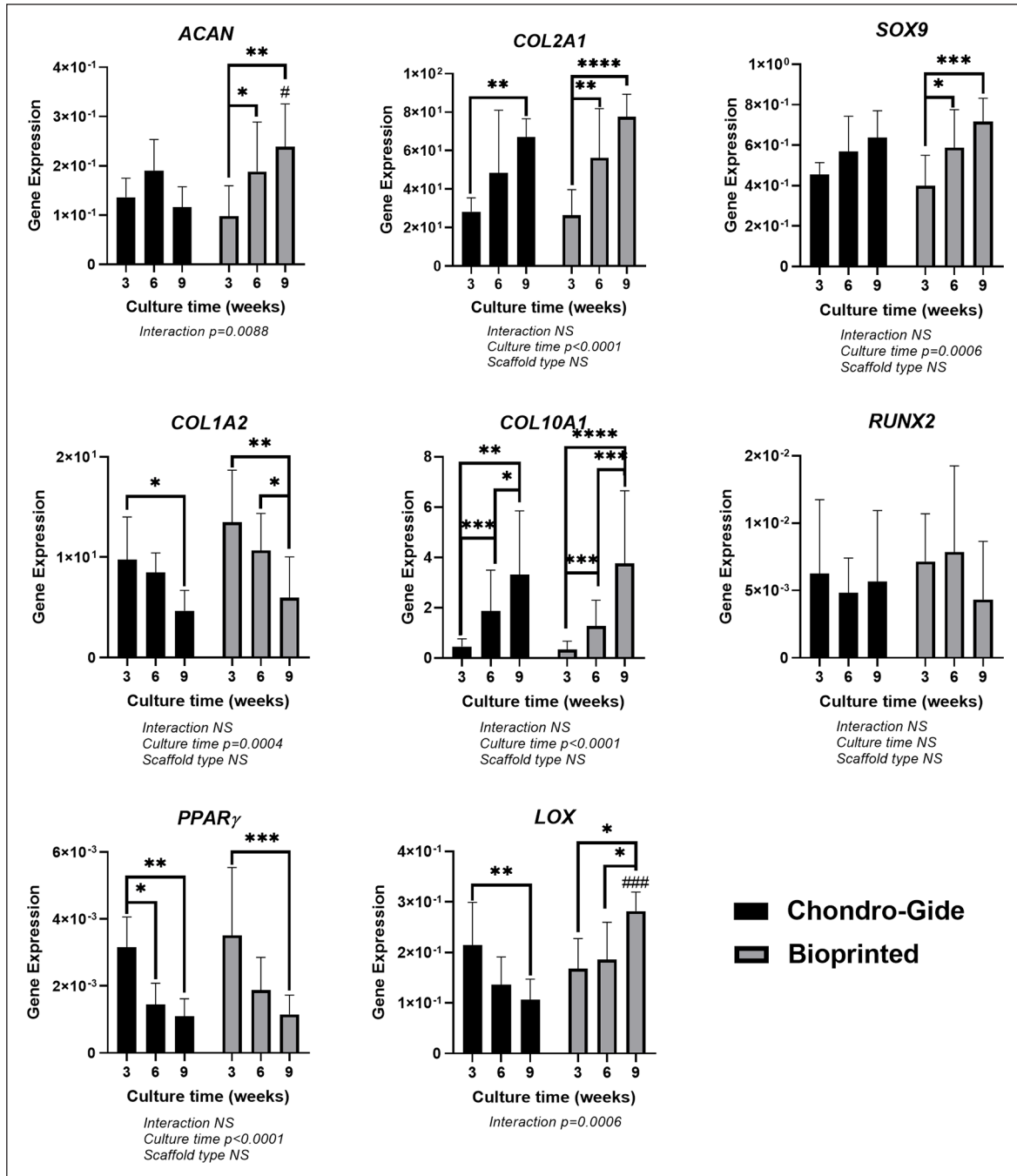


**Figure 8.** Gene expression of in vitro constructs. Values shown are  $2^{-\Delta\text{Ct}}$  values from RT-qPCR. Statistics were done using  $\Delta\text{Ct}$  values. Data was analyzed by two-way ANOVA and corrected with the Bonferroni post hoc test. Housekeeping genes used were ACTB, B2M, and YWHAZ.  $n=6$  donors (in duplicate). NS: non-significant. Star (\*) represent the significant difference with regarding of culture time after Bonferroni post hoc correction: \* represents  $0.01 < p < 0.05$ , \*\* represents  $0.001 < p < 0.01$ , \*\*\* represents  $0.0001 < p < 0.001$ , \*\*\*\* represents  $p < 0.00001$ . Pound (#) represent the significant difference with regarding of scaffold type after Bonferroni post hoc correction: # represents  $0.01 < p < 0.05$ , ### represents  $0.0001 < p < 0.001$ .

(*COL10A1*), osteogenic (*RUNX2*), and adipogenic genes (*PPAR $\gamma$* ). Additionally, the expression of the collagen cross linking enzyme (*LOX*) was quantified as well. The results were analyzed by two-way ANOVA and corrected with Bonferroni post hoc tests.

The expression of chondrogenic-related genes was all found to be affected by culture time. Only *ACAN* expression was shown to have a significant interaction between scaffold type and culture time ( $p=0.0088$ , Figure 8). For bioprinted constructs, the expression of *ACAN* was found

to increase with increasing culture time, with significant differences in expression between 3 and 6 weeks, 3 and 9 weeks. However, for Chondro-Gide scaffolds, *ACAN* expression was found to increase only from 3 to 6 weeks and then decrease from 6 to 9 weeks (no significant differences). A significant difference was found at 9 weeks between bioprinted construct and Chondro-Gide *ACAN* expression. Both the expression of *COL2A1* and *SOX9* were significantly affected by culture time ( $p < 0.0001$ – $p = 0.0006$ , respectively), as the expression for both genes increased with increasing culture time. *COL1A2* expression was also significantly affected by culture time ( $p = 0.0004$ ), but instead, expression decreased with increasing culture time. There were no significant differences in *COL2A1*, *SOX9*, and *COL1A2* expressions between bioprinted constructs and Chondro-Gide scaffolds. The expression of *COL10A1* was significantly upregulated as the culture time increased ( $p < 0.0001$ ), with no significant differences between scaffold types. There was also a significant decrease in *PPAR $\gamma$*  expression ( $p < 0.0001$ ) with culture time, with no significant differences between scaffold types. A significant interaction was also found between scaffold type and culture time for *LOX* ( $p = 0.0006$ ). For bioprinted constructs and Chondro-Gide scaffolds, the expression of *LOX* was shown to increase and decrease significantly with culture time, respectively. The expression of *RUNX2* was not affected by either culture time or scaffold type.

### Gross morphology of engineered cartilages after *in vivo* implantation in nude mice

Following implantation in nude mice, the gross morphologies of the engineered cartilages were assessed for macroscopic differences. After 5 weeks of implantation, both bioprinted constructs and Chondro-Gide scaffolds maintained their original size and shape (Figure 9(a)). Both engineered cartilages were smooth and opaque following *in vivo* culture compared to the gluey and formless appearance of non-precultured engineered cartilages (empty scaffolds).

### Histology and immunofluorescence after *in vivo* implantation

To characterize the nature of the ECM following implantation, Safranin-O and Masson's trichrome staining were performed to assess and compare the matrix composition of *in vivo* cultured engineered cartilages to *in vitro* controls. Following *in vivo* culture, both cell-laden bioprinted constructs and Chondro-Gide scaffolds showed peripheral loss of proteoglycan-rich matrix, denoted by the loss of Safranin-O staining (Figure 10, all the explanted donors are shown in Supplemental Figure S7). The intensity of Safranin-O staining was overall fainter in the *in vivo*

cartilages compared to the *in vitro* cartilages. No matrix deposition was observed in empty scaffolds. Collagen deposition, denoted by aniline blue, was slightly different between *in vitro* and *in vivo* cartilages. Engineered cartilages implanted *in vivo* appeared to have a more intense collagen staining in the periphery that contrasted Safranin-O staining, like native tissue. However, *in vitro* cartilages appeared to have a more diffuse and generalized distribution of collagen staining. Bioprinted constructs overall had more collagen staining than Chondro-Gide in both the *in vitro* and *in vivo* conditions. Collagen deposition that was observed in both empty scaffolds was most likely due to mouse skin cell infiltration, which is supported by the presence of cell nuclei and lack of human specific collagen expression detected by immunofluorescence (Figure 10). To characterize and compare the collagen deposition in the *in vivo* cultured engineered cartilages to those cultured *in vitro*, types I and II collagen immunofluorescence were performed. The expression of type I and II collagens were shown to be maintained in the cell-laden engineered cartilages following *in vivo* culture (all the explanted donors are shown in Supplemental Figure S8), with type II collagen expression being the most pronounced. Type II collagen expression was also more intense in *in vivo* than *in vitro* cartilages. To determine whether macrophages contributed to the loss of the proteoglycan-rich matrix *in vivo*, BM8 immunofluorescence was performed (Supplemental Figure S10). Macrophages were observed in both *in vivo* cultured engineered cartilages, suggesting a phagocytic role of macrophages in proteoglycan loss. To assess the extent of bone formation in the *in vivo* cartilages, a few different analyses were performed. CD31, BSP, type  $\times$  collagen immunofluorescence, and Alizarin Red S staining were performed to detect blood vessel invasion, bone ossification, chondrocyte hypertrophy, and calcium deposition in the *in vivo* cartilages, respectively. There was no evidence of blood vessel invasion, bone growth, or mineralization in either the cell-laden bioprinted constructs or Chondro-Gide scaffolds (Figure 9(b), Alizarin Red S for explanted scaffolds and native tissue are shown in Supplementary Figure S9). Empty scaffolds implanted *in vivo* showed some evidence of blood vessel invasion. *In vitro* parallel-cultured engineered cartilages served as a negative control for both BSP and Alizarin Red S staining. Type  $\times$  collagen expression was observed in both bioprinted constructs and Chondro-Gide scaffolds *in vivo*, however, this staining was like *in vitro* controls.

### Mechanical property after *in vivo* implantation

To assess the effects of *in vivo* culture on the mechanical properties of engineered cartilages, a three-point bending test was performed before and after implantation in nude mice. Bending modulus was shown to increase from

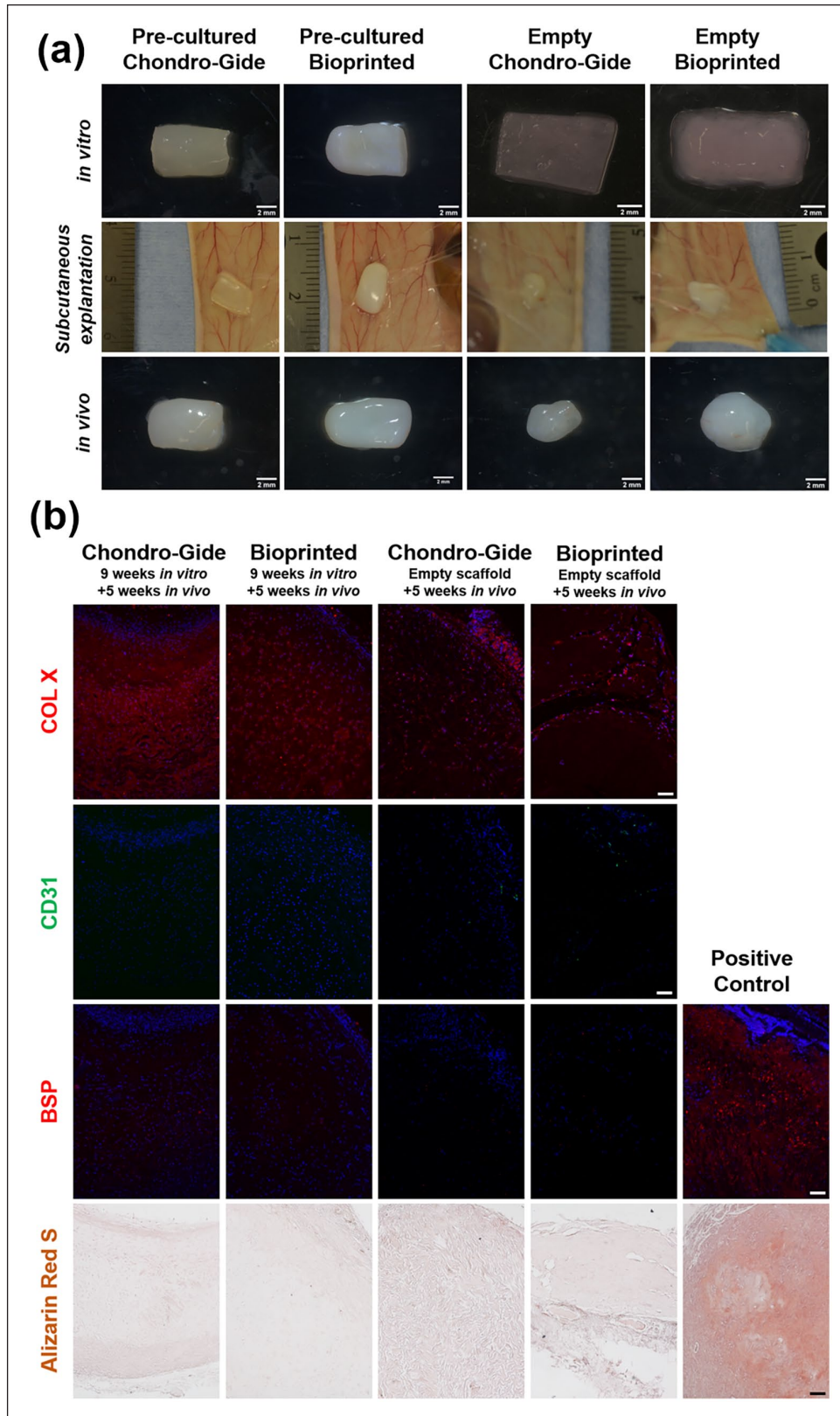


**Figure 9.** (a) Gross morphology of constructs and scaffolds before and after implantation. (b) Histology and immunofluorescence of in vivo bone formation proteins, including type X collagen (red represents positive type X collagen, which is a marker of chondrocyte hypertrophy), CD31 (green represents positive CD31, CD31 is a marker of angiogenesis), BSP (red represents positive bone sialoprotein formation), and Alizarin Red S (orange color represents positive calcification). COL10; type X collagen, CD31; cluster of differentiation 31, BSP; bone sialoprotein. Scale bar: 100  $\mu$ m.

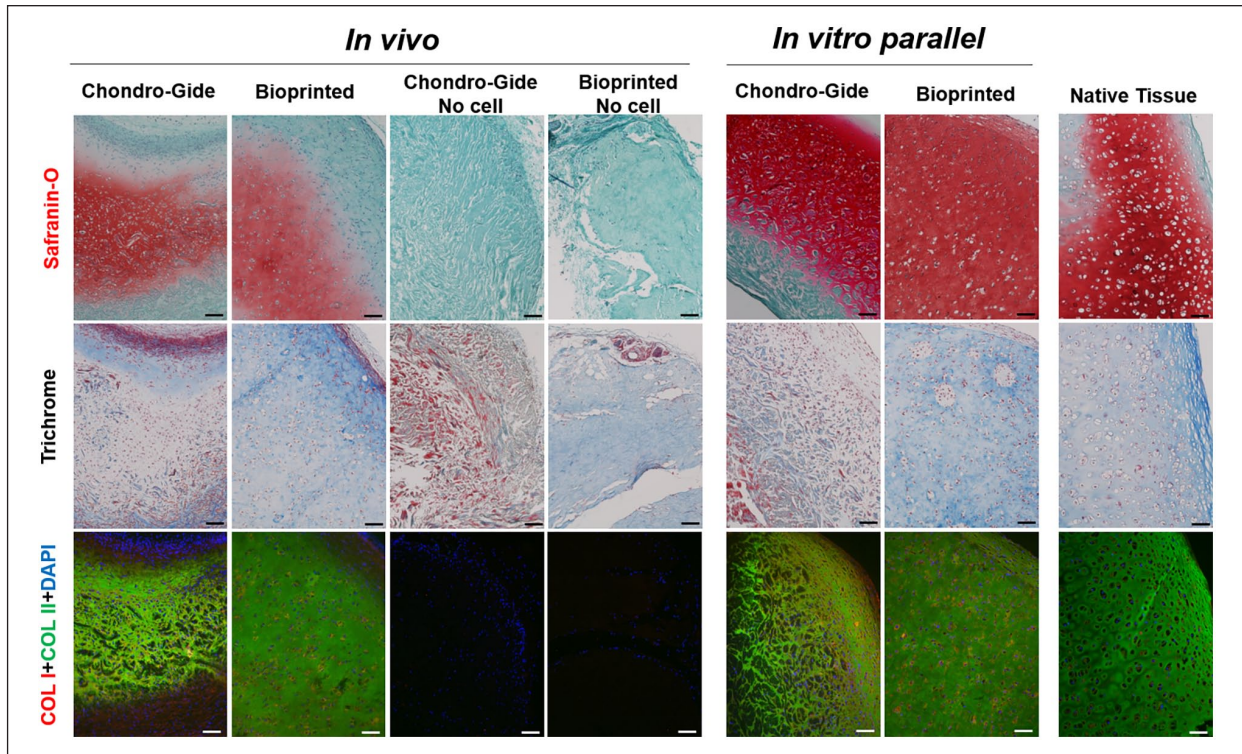


**Figure 10.** Histology and immunofluorescence of chondrogenic related proteins, including Safranin-O/Fast Green staining, Masson's Trichrome staining, and type I and II collagens immunofluorescence. Scale bar: 100  $\mu$ m.

$0.287 \pm 0.0513$  to  $0.534 \pm 0.189$  MPa in Chondro-Gide and from  $0.298 \pm 0.577$  to  $0.582 \pm 0.0444$  Pa in bioprinted constructs. All three donors showed an increase in bending modulus after implantation. The size of the implanted Donor #1 is untestable due to the size limitation.

## Discussion

In this study, we have used human nasoseptal chondrocytes (hNC)-laden bovine type I collagen hydrogel to 3D bioprint engineered nasal human cartilage. Our results supported the biofabrication of a robust and mechanically suturable engineered human nasal cartilage that is comparable if not better than engineered human nasal cartilage graft from hNC-seeded porcine type I and III collagen membrane scaffold, Chondro-Gide. The bioprinted tissue was characterized by increased cellular viability from the time of biofabrication to the endpoint of 9 weeks of *in vitro* tissue development at which point there was a fall in the measured cellular viability relative to 3- and 6-week time points. The reason for the decline is unclear but the majority of the cells' morphology at 9 weeks seem to be consistent with the adhesive model of cell migration in 3D collagen lattices, suggesting that a number of cells may have migrated out of the engineered tissue construct after the 9 weeks long of ECM accumulation and matrix remodeling.<sup>38</sup> However, this would need to be verified in future studies.

Furthermore, our results emphasize the capacity of the extensively cell culture expanded hNCs, up to six cell population doublings, in cell growth media supplemented with TGF- $\beta$ 1 and FGF-2 of been able to synthesize and organize cartilage ECM within the hNCs-laden type I collagen hydrogel for bioprinting and within the type I/III collagen membrane scaffold. These results are consistent with our previous works<sup>13,22</sup> and Fulco et al.'s<sup>3</sup> work using the collagen membrane scaffold. Since the functional component of cartilage is its ECM,<sup>39</sup> we evaluated the progression of tissue maturation over time. After 3, 6, 9 weeks of chondrogenic culture, we first analyzed for cartilaginous ECM formation by visualizing sulfated proteoglycan via Safranin-O staining, collagen deposition via Masson Trichrome staining, human types I and II collagen via immunofluorescence (Figure 4(a, b) and 5(a)). The bioprinted constructs showed a uniform distribution of Safranin O positive, collagen, and human types I/II collagen distribution relative to the same ECM distribution in the porcine-derived type I/III collagen membrane scaffolds. Thus, one benefit of the bioprinting approach for fabrication of the engineered nasal cartilage graft is that it allowed the hNCs to be homogeneously distributed within the bovine-derived type I collagen hydrogel before the 3D layer-by-layer deposition of the hNCs-laden hydrogel. In contrast, the distribution of the hNCs synthesized cartilaginous ECM appeared to be less uniformly distributed and restricted to the porous layer of the

porcine-derived type I/III collagen membrane scaffold albeit with some evidence of the ECM extending into the smooth compact layer of the membrane over the course of the in vitro tissue maturation.

Quantitative measures of the chondrogenic capacity (i.e. GAG/DNA) of the hNCs within the two matrices used in this study supports the superiority of the microenvironment of the hydrogel in facilitating the chondrogenic redifferentiation of the hNCs. The GAG/DNA values for the bioprinted engineered nasal cartilage were higher than in the porcine-derived type I/III collagen membrane scaffolds with magnitudes of 14.38, 13.74, 12.48  $\mu\text{g}/\mu\text{g}$  for 3, 6, 9 weeks, respectively. This superiority is consistent with reports that the branched network of loose bundles of collagen fibers as found in collagen hydrogels as supposed to the membrane-like flatten wall internal structure of the fibers presented in the porous collagen sponges supports the round chondrocytic phenotype of chondrocytes.<sup>40-42</sup> However, it is interesting to note that while the chondrogenic capacity of the hNCs within the hydrogel matrix was superior relative to the collagen membrane scaffold, the gene expression of types I and X collagen were not different between the hydrogel and membrane scaffold as previously reported between the different internal structures of chitosan-based scaffold forms of sponges and hydrogels.<sup>40</sup> To that end, our finding seems to suggest that both the internal structure and composition of scaffolds play a role in the phenotypic expression of the cells in any given scaffold. The higher GAG/DNA contents in collagen I bioink group may be attributed to a superior display of synthetic capacity of the hNCs within the hydrogel microenvironment as well the entrapment of the synthesized ECM within the hydrogel matrix.

Given the fact that the mechanical strength of cartilaginous structures is by reason of their ECM's composition and organizational structure, it is no surprise that as the ECM synthesized by the hNCs increased and accumulated with in vitro culture duration within the bioprinted constructs that it played a vital role in the development of its tensile properties (Figure 6(a)). As the images (Figure 6(a)) demonstrate, after 3 weeks of culture, the bioprinted constructs were unable to hold surgical sutures an indication of a weak tensile strength. However, it was not until after 9 weeks of in vitro culture that the bioprinted constructs' tensile properties was adequate to hold the surgical sutures without failure. In contrast, the high tensile strength of the collagen membrane was adequate to hold surgical sutures regardless of the in vitro culture duration of the due to the arrangement of its collagen fibers.<sup>3</sup> It is interesting to note that the ultrastructure of native human septal cartilage and that of the collagen membrane-derived engineered nasal cartilage looked very similar regardless of the in vitro culture maturation time with obvious tightly organized collagen fibers, while porous spaces are evident in the bioprinted constructs of engineered cartilage at 3 and

6 weeks but not at the 9 weeks culture time when the ultrastructure looked similar to the ultrastructure of the native septal cartilage and collagen membrane-derived engineered cartilage. To that end, it is reasonable to speculate that the subsequent filling or remodeling of the spaces contributed to the augmented tensile strength of the bioprinted construct after 9 weeks. The increased lysyl oxidase (*LOX*) expression which relatively peaked at 9 weeks coincided the improved tensile strength (Figure 8). Thus, given *LOX*'s functionality in crosslinking collagen and improving mechanical strength of engineered cartilage, we speculate that *LOX* contributed to the augmented tensile strength after the 9 weeks of maturation.<sup>43,44</sup> The mechanism underlying the observed upregulation of *LOX* in the bioprinted constructs and its decline in the collagen membrane-derived constructs is unclear but may be associated with alterations in local hypoxia microenvironment as the cartilaginous ECM is deposited and remodeled within the cell-laden constructs. Makris et al has shown that *LOX* expression could be induced through hypoxia.<sup>43</sup> One possibility is a limited access of the hNCs-media contact in the compact layer of the collagen membrane scaffold which may have led to a local hypoxic environment, resulting in a higher *LOX* gene expression at 3 weeks. However, as culture time increased, the de novo synthesized and deposited ECM by the hNCs remodeled with extension into the compact layer leading to a disruption of the local hypoxic microenvironment with concomitant decline in *LOX* gene expression. In contrast, the hNCs within the bioprinted hydrogel constructs had high initial cell-media contact that permitted a homogenous access of media dissolved oxygen to the hNCs. But as the hNCs within the bioprinted construct synthesized, deposited, and remodeled the de novo ECM during maturation local hypoxic microenvironments emerged leading to increased *LOX* expression.

In addition to the bioprinted engineered cartilage improved tensile characteristics as judged by its suturability, the bending modulus of the bioprinted cartilage experienced a larger increase with culture maturation time than the collagen membrane-derived engineered cartilage constructs. This finding further supports the concept that the gradual improvement in the tensile strength and suturability of the bioprinted engineered cartilage aligned with increased ECM production and accumulation within the hydrogel scaffold.

Monolayer expanded chondrocytes expressed adipogenic, chondrogenic, and osteogenic markers genes and encoded proteins after respective inductions.<sup>45,46</sup> Therefore, we investigated the expression of adipogenic, chondrogenic, and osteogenic marker genes to assess in vitro phenotypic stability of the chondrogenically stimulated monolayer-expanded hNCs. Our findings showed a gradual decline in adipogenic (*PPAR $\gamma$* ) and fibrogenic (*COL1A2*) marker gene expression regardless of whether



**Table 3.** Bending modulus before and after implantation.

Scaffold type	Before implantation (Pa)			After implantation (Pa)		
	21/M Donor #1	30/M Donor#3	48/M Donor#6	21/M Donor #1	30/M Donor#3	48/M Donor#6
Chondro-Gide	227,627	312,329	320,105	448,666	751,396	402,828
Bioprinted	248,587	284,047	361,490	N/A	549,189	611,978

the collagen membrane or hydrogel scaffold was used during in vitro maturation of the engineered cartilage constructs. In contrast, chondrogenic markers' gene expression (*COL2A1*, *SOX9*, *ACAN*) increased with culture time in the cell-laden hydrogel bioprinted constructs and to some extent similarly in the collagen membrane albeit with a notable drop in *ACAN* expression at 9 weeks. These results further reinforce the superiority of the hydrogel microenvironment in the enhancing the chondrogenic phenotype of the chondrogenically stimulated monolayer-expanded hNCs.

The expression of *COL10A1*, a marker of hypertrophic chondrocyte has been shown to correlate with the propensity of chondrogenically induced bone marrow mesenchymal stem cells to undergo transformation akin to endochondral ossification.<sup>47</sup> As such, we investigated the expression of *COL10A1* and observed its upregulation with culture maturation time in both the cell-laden bioprinted and the collagen membrane constructs. Furthermore, its encoded protein, type X collagen, was evident via immunofluorescence in the constructs (Figure 5(b)). To ensure that the engineered cartilage constructs were stable phenotypically in vivo without the risk of undergoing ossification, the constructs after 9 weeks of in vitro maturation were subcutaneously implanted in immunodeficient nude mice. There was no evidence of ossification regardless of whether the engineered cartilage construct was bioprinted or collagen membrane-derived after 5 weeks of implantation in the mice. This finding was consistent with our previous findings in regard to engineered cartilage in the collagen membrane scaffold.<sup>13</sup> Interestingly, Aksoy et al.<sup>48</sup> showed native nasal septal cartilage contain small amounts of Type X collagen. Thus, it is reasonable to speculate that compositionally our engineered cartilage constructs resemble native nasoseptal cartilage.

In vivo preservation of the engineered cartilage constructs poses several challenges: the shrinkage and deformation of the construct due to the skin tension,<sup>49-51</sup> the calcification of tissue-engineered cartilage,<sup>13,47,49,52</sup> and the preservation of cartilage-like ECM after implantation.<sup>14</sup> In this study, the bioprinted constructs were able to maintain their gross morphology even after 5 weeks of implantation. However, the gross morphology of the cell-free scaffolds deformed and shrunk suggesting some sort of remodeling or cell-mediated contraction had taken place (Figure 9). Following other histological and immunofluorescence

assessments in addition to the above-mentioned assessment for bone formation after in vivo implantation, positive CD31 fluorescence were evident in the cell-free scaffolds suggesting an invasion of endothelial cells which may contributed to the observed shrinkage through cell-mediated contraction of the scaffold. Moreover, Safranin-O positive ECM staining was notably reduced after in vivo implantation, but the fluorescence of types I and II collagen remained unchanged as prior to in vivo implantation. These findings are consistent with previous studies of implanted engineered nasal cartilages.<sup>13,53</sup> But it is unclear the underlying mechanism of the decline of the Safranin O positive ECM. We reasoned it could be due to macrophage invasion from the nude mouse.<sup>54-56</sup> Thus, we assessed the presence of macrophage with anti-F4/80, a unique marker of murine macrophages in the explanted tissue engineered constructs,<sup>57</sup> the F4/80 immunofluorescent results are shown in Supplemental Figure S10. The assessment proved positive for the presence of macrophages and supported the mechanistic possibility that the decline of the Safranin O positive ECM may have been mediated by macrophage secreted matrix metalloproteinases as previously reported.<sup>56,58,59</sup>

The mechanical strength of both engineered cartilage constructs increased almost two-fold after in vivo implantation as shown in Table 3. This finding suggested that the constructs underwent further remodeling or maturation in vivo after 9 weeks of in vitro maturation. This finding therefore raises the question; what is an adequate duration for in vitro maturation of engineered cartilage to achieve mechanical robustness for surgical handling prior to reconstructive surgery? Previous work, albeit in articular cartilage repair, indicated that 2 weeks of in vitro maturation of engineered cartilage resulted in better integrative repair relative to 6 weeks of in vitro maturation.<sup>60</sup> To this end, it is reasonable to suggest that a timeframe that enables suturability or mechanical handling during reconstructive surgery is appropriate given that further in vivo maturation is inevitable.

A potential limitation of our study was that only male donors were included which was due to the limited donor supply from the hospital. Previous research has not shown any significant differences between males and females in terms of nasal cartilage compositions and shapes.<sup>61,62</sup> A pilot study might be worth future investigation to compare the effects of sex on the compositions of engineered cartilage tissues.

## Conclusion

This study demonstrated the perspective of bioprinting engineered cartilage grafts with similar histological, molecular, and mechanical characteristics as those derived from the use of clinically approved type I/III collagen membrane scaffolds both in vivo and in vitro. Moreover, the mechanical characteristics of the bioprinted engineered grafts increased after in vivo implantation. Overall, this study showed strong evidence of the potential to engineer human nasal cartilage grafts for nasal reconstructive surgery via 3D bioprinting.

## Acknowledgements

We are grateful for the donation of the type I/III collagen membrane scaffold, Chondro-Gide, from Geistlich Pharma AG, Switzerland. We would like to thank the surgeons from Division of Otolaryngology and associated operating room nurses at the University Hospital of Alberta (Edmonton, Alberta), Grey Nuns Community Hospital (Edmonton, Alberta), and the Leduc Community Hospital (Leduc, Alberta) for assistance with procurement of human nasal septal tissue specimens. We acknowledge the staff in the Scanning Electron Microscope Laboratory in the Department Earth and Atmospheric Sciences, University of Alberta for taking the SEM images. We acknowledge the help of the Cell Imaging Center in the Faculty of Medicine and Dentistry, University of Alberta for the use of the confocal microscope. The schematic diagram is created with BioRender.com. We acknowledge Zhiyao (Hilda) Ma in Prof. Adetola Adesida's lab for writing the algorithm to quantify the immunofluorescence intensity and cell number using python.

## Author contributions

XL conducted the experiments and was responsible for experimental design, data acquisition, analysis, and manuscript writing. YL and MK contributed to the animal surgery. MV contributed to the manuscript writing. EJNE, MV, MK, and AMS were involved in immunofluorescence, gene expression, and cell culture. MO, KA, and HS involved in nasal cartilage procurement, and review. YB was involved in supervision and final manuscript review. ABA conceived and supervised the study, was responsible for writing and final review of the manuscript. All authors read and approved the final manuscript.

## Availability of data and materials

The original contributions presented in the study are included in the article/Supplementary Materials, and further inquiries can be directed to the corresponding author.

## Declaration of conflicting interests

The author(s) declared no potential conflicts of interest with respect to the research, authorship, and/or publication of this article.

## Funding

The author(s) disclosed receipt of the following financial support for the research, authorship, and/or publication of this article:

Financial support was provided by Canadian Institutes for Health Research (CIHR PS 159,661) to ABA, MO, KA, and HS, Alberta Cancer Foundation-Mickleborough Interfacial Biosciences Research Program (ACF-MIBRP 27,128) to ABA, MO, and KA, Edmonton Civic Employees Charitable Assistance Fund (RES0041788) to XL, YB, and ABA, Natural Sciences and Engineering Research Council of Canada – Discovery Grant Program (NSERC RGPIN 06431) to YB, Canadian Foundation for Innovation (CFI 33786) to ABA, University Hospital Foundation (RES0028185) to ABA.

## ORCID iDs

Margaret Vyhlidal  <https://orcid.org/0000-0002-9972-9226>

Adetola B Adesida  <https://orcid.org/0000-0003-1798-6251>

## Supplemental material

Supplemental material for this article is available online.

## References

- Madan V, Lear JT and Szeimies R-M. Non-melanoma skin cancer. *Lancet* 2010; 375: 673–685.
- Lomas A, Leonardi-Bee J and Bath-Hextall F. A systematic review of worldwide incidence of nonmelanoma skin cancer. *Br J Dermatol* 2012; 166: 1069–1080.
- Fulco I, Miot S, Haug MD, et al. Engineered autologous cartilage tissue for nasal reconstruction after tumour resection: an observational first-in-human trial. *Lancet* 2014; 384: 337–346.
- Austin GK and Shockley WW. Reconstruction of nasal defects: contemporary approaches. *Curr Opin Otolaryngol Head Neck Surg* 2016; 24: 453–460.
- Burget GC and Menick FJ. The subunit principle in nasal reconstruction. *Plast Reconstr Surg* 1985; 76: 239–247.
- Menick FJ. Nasal reconstruction. *Plast Reconstr Surg* 2010; 125: 138e–150e.
- Sajjadian A, Naghshineh N and Rubinstein R. Current status of grafts and implants in rhinoplasty: Part II. Homologous grafts and allogenic implants. *Plast Reconstr Surg* 2010; 125: 99e–109e.
- Menger DJ and Nolst Trenité GJ. Irradiated homologous rib grafts in nasal reconstruction. *Arch Facial Plast Surg* 2010; 12: 114–118.
- Wee JH, Mun SJ, Na WS, et al. Autologous vs irradiated homologous costal cartilage as graft material in rhinoplasty. *JAMA Facial Plast Surg* 2017; 19: 183–188.
- Patel K and Brandstetter K. Solid implants in facial plastic surgery: potential complications and how to prevent them. *Facial Plast Surg* 2016; 32: 520–531.
- Farkas JP, Lee MR, Lakianhi C, et al. Effects of carving plane, level of harvest, and oppositional suturing techniques on costal cartilage warping. *Plast Reconstr Surg* 2013; 132: 319–325.
- Lavernia L, Brown WE, Wong BJB, et al. Toward tissue-engineering of nasal cartilages. *Acta Biomater* 2019; 88: 42–56.
- Andrews SHJ, Kunze M, Mulet-Sierra A, et al. Strategies to mitigate variability in engineering human nasal cartilage. *Sci Rep* 2017; 7: 6490.

14. Farhadi J, Fulco I, Miot S, et al. Precultivation of engineered human nasal cartilage enhances the mechanical properties relevant for use in facial reconstructive surgery. *Ann Surg* 2006; 244: 978–985.
15. Mumme M, Barbero A, Miot S, et al. Nasal chondrocyte-based engineered autologous cartilage tissue for repair of articular cartilage defects: an observational first-in-human trial. *Lancet* 2016; 388: 1985–1994.
16. Yi H-G, Choi Y-J, Jung JW, et al. Three-dimensional printing of a patient-specific engineered nasal cartilage for augmentative rhinoplasty. *J Tissue Eng* 2019; 10: 2041731418824797.
17. Vinatier C, Gauthier O, Masson M, et al. Nasal chondrocytes and fibrin sealant for cartilage tissue engineering. *J Biomed Mater Res* 2009; 89: 176–185.
18. Murphy SV and Atala A. 3D bioprinting of tissues and organs. *Nat Biotechnol* 2014; 32: 773–785.
19. Murphy SV, Skardal A and Atala A. Evaluation of hydrogels for bio-printing applications. *J Biomed Mater Res A* 2013; 101: 272–284.
20. Nakamura M, Iwanaga S, Henmi C, et al. Biomatrices and biomaterials for future developments of bioprinting and bio-fabrication. *Biofabrication* 2010; 2: 014110.
21. Mandrycky C, Wang Z, Kim K, et al. 3D bioprinting for engineering complex tissues. *Biotechnol Adv* 2016; 34: 422–434.
22. Lan X, Liang Y, Erkut EJN, et al. Bioprinting of human nasoseptal chondrocytes-laden collagen hydrogel for cartilage tissue engineering. *FASEB J* 2021; 35: e21191.
23. Ruiz-Cantu L, Gleadall A, Faris C, et al. Multi-material 3D bioprinting of porous constructs for cartilage regeneration. *Mater Sci Eng C* 2020; 109: 110578.
24. Kundu J, Shim JH, Jang J, et al. An additive manufacturing-based PCL-alginate-chondrocyte bioprinted scaffold for cartilage tissue engineering. *J Tissue Eng Regen Med* 2015; 9: 1286–1297.
25. Martínez Ávila H, Schwarz S, Rotter N, et al. 3D bioprinting of human chondrocyte-laden nanocellulose hydrogels for patient-specific auricular cartilage regeneration. *Bioprinting* 2016; 1–2: 22–35.
26. Apelgren P, Amoroso M, Lindahl A, et al. Chondrocytes and stem cells in 3D-bioprinted structures create human cartilage in vivo. *PLoS One* 2017; 12: e0189428.
27. Apelgren P, Amoroso M, Säljö K, et al. Skin grafting on 3D bioprinted cartilage constructs in vivo. *Plast Reconstr Surg Glob Open* 2018; 6: e1930.
28. Markstedt K, Mantas A, Tournier I, et al. 3D bioprinting human chondrocytes with nanocellulose-alginate bioink for cartilage tissue engineering applications. *Biomacromolecules* 2015; 16: 1489–1496.
29. Gu Y, Schwarz B, Forget A, et al. Advanced bioink for 3D bioprinting of complex free-standing structures with high stiffness. *Bioengineering* 2020; 7: 141.
30. Möller T, Amoroso M, Hägg D, et al. In vivo chondrogenesis in 3D bioprinted human cell-laden hydrogel constructs. *Plast Reconstr Surg Glob Open* 2017; 5: e1227.
31. Liang Y, Idrees E, Szojka ARA, et al. Chondrogenic differentiation of synovial fluid mesenchymal stem cells on human meniscus-derived decellularized matrix requires exogenous growth factors. *Acta Biomater* 2018; 80: 131–143.
32. Sabiston P, Adams ME and Ho YA. Automation of 1,9-dimethylmethylene blue dye-binding assay for sulfated glycosaminoglycans with application to cartilage microcultures. *Anal Biochem* 1985; 149: 543–548.
33. Lee AS, Rusch J, Lima AC, et al. Rare mutations in the complement regulatory gene CSMD1 are associated with male and female infertility. *Nat Commun* 2019; 10: 4626.
34. Liang Y, Idrees E, Andrews SHJ, et al. Plasticity of human meniscus fibrochondrocytes: a study on effects of mitotic divisions and oxygen tension. *Sci Rep* 2017; 7: 12148.
35. Grogan SP, Barbero A, Winkelmann V, et al. Visual histological grading system for the evaluation of in vitro-generated neocartilage. *Tissue Eng* 2006; 12: 2141–2149.
36. Allen RE, Masak KC and McAllister PK. Staining protein in isoelectric focusing gels with fast green. *Anal Biochem* 1980; 104: 494–498.
37. Dey P. Connective tissue stain: principle and procedure. In: *Basic and advanced laboratory techniques in histopathology and cytology*. Singapore: Springer, 2018, pp.99–108.
38. Friedl P, Zänker KS and Bröcker EB. Cell migration strategies in 3-D extracellular matrix: differences in morphology, cell matrix interactions, and integrin function. *Microsc Res Tech* 1998; 43: 369–378.
39. Fisch P, Broguiere N, Finkielstein S, et al. Bioprinting of cartilaginous auricular constructs utilizing an enzymatically crosslinkable bioink. *Adv Funct Mater* 2021; 31 (16): 2008261.
40. Zhang J, Yang Z, Li C, et al. Cells behave distinctly within sponges and hydrogels due to differences of internal structure. *Tissue Eng Part A* 2013; 19: 2166–2175.
41. Chao PHG, Yodmuang S, Wang X, et al. Silk hydrogel for cartilage tissue engineering. *J Biomed Mater Res Part B Appl Biomater* 2010; 95: 84–90.
42. Benya PD and Shaffer JD. Dedifferentiated chondrocytes reexpress the differentiated collagen phenotype when cultured in agarose gels. *Cell* 1982; 30: 215–224.
43. Makris EA, Responte DJ, Paschos NK, et al. Developing functional musculoskeletal tissues through hypoxia and lysyl oxidase-induced collagen cross-linking. *Proc Natl Acad Sci USA* 2014; 111: E4832–E4841.
44. Makris EA, Hu JC and Athanasiou KA. Hypoxia-induced collagen crosslinking as a mechanism for enhancing mechanical properties of engineered articular cartilage. *Osteoarthr Cartil* 2013; 21(4): 634–641.
45. Vinod E, Kachroo U, Amirtham SM, et al. Comparative analysis of fresh chondrocytes, cultured chondrocytes and chondroprogenitors derived from human articular cartilage. *Acta Histochem* 2020; 122: 151462.
46. Barbero A, Ploegert S, Heberer M, et al. Plasticity of clonal populations of dedifferentiated adult human articular chondrocytes. *Arthritis Rheum* 2003; 48: 1315–1325.
47. Pelttari K, Winter A, Steck E, et al. Premature induction of hypertrophy during in vitro chondrogenesis of human mesenchymal stem cells correlates with calcification and vascular invasion after ectopic transplantation in SCID mice. *Arthritis Rheum* 2006; 54: 3254–3266.
48. Aksoy F, Yildirim YS, Demirhan H, et al. Structural characteristics of septal cartilage and mucoperichondrium. *J Laryngol Otol* 2012; 126: 38–42.

49. Bomhard AV, Veit J, Bermueller C, et al. Prefabrication of 3D cartilage constructs: towards a tissue engineered auricle: a model tested in rabbits. *PLoS One* 2013; 8: e71667.
50. Zhou L, Pomerantseva I, Bassett EK, et al. Engineering ear constructs with a composite scaffold to maintain dimensions. *Tissue Eng Part A* 2011; 17: 1573–1581.
51. Liao HT, Zheng R, Liu W, et al. Prefabricated, ear-shaped cartilage tissue engineering by scaffold-free porcine chondrocyte membrane. *Plast Reconstr Surg* 2015; 135: 313e–321e.
52. Pippenger BE, Ventura M, Pelttari K, et al. Bone-forming capacity of adult human nasal chondrocytes. *J Cell Mol Med* 2015; 19: 1390–1399.
53. Anderson-Baron M, Liang Y, Kunze M, et al. Suppression of hypertrophy during in vitro chondrogenesis of cocultures of human mesenchymal stem cells and nasal chondrocytes correlates with lack of in vivo calcification and vascular invasion. *Front Bioeng Biotechnol* 2020; 8: 572356.
54. Bucana CD, Fabra A, Sanchez R, et al. Different patterns of macrophage infiltration into allogeneic-murine and xenogeneic-human neoplasms growing in nude mice. *Am J Pathol* 1992; 141: 1225–1236.
55. Fujihara Y, Asawa Y, Takato T, et al. Tissue reactions to engineered cartilage based on poly-L-lactic acid scaffolds. *Tissue Eng Part A* 2009; 15: 1565–1577.
56. Janusz MJ, Hare M, Durham SL, et al. Cartilage proteoglycan degradation by a mouse transformed macrophage cell line is mediated by macrophage metalloelastase. *Inflamm Res* 1999; 48: 280–288.
57. Dos Anjos Cassado A. F4/80 as a major macrophage marker: the case of the peritoneum and spleen. *Results Probl Cell Differ* 2017; 62: 161–179.
58. Kraus VB, McDaniel G, Huebner JL, et al. Direct in vivo evidence of activated macrophages in human osteoarthritis. *Osteoarthr Cartil* 2016; 24: 1613–1621.
59. Raghu H, Lepus CM, Wang Q, et al. CCL2/CCR2, but not CCL5/CCR5, mediates monocyte recruitment, inflammation and cartilage destruction in osteoarthritis. *Ann Rheum Dis* 2016; 76: 914–922.
60. Miot S, Brehm W, Dickinson S, et al. Influence of in vitro maturation of engineered cartilage on the outcome of osteochondral repair in a goat model. *Eur Cell Mater* 2012; 23: 222–236.
61. Homicz MR, McGowan KB, Lottman LM, et al. A compositional analysis of human nasal septal cartilage. *Arch Facial Plast Surg* 2003; 5: 53–58.
62. Kim I-S, Lee M-Y, Lee K-I, et al. Analysis of the development of the nasal septum according to age and gender using MRI. *Clin Exp Otorhinolaryngol* 2008; 1: 29.